Contribution from the Department of Chemistry,
University of Durham, Durham, United Kingdom DH1 3LE

Anodic Electrodeposition of Thin Films of Polypyrrole Functionalized with Metal Bipyridyl Redox Centers

Jeffrey G. Eaves, Hugh S. Munro, and David Parker*

Received August 4, 1986

Anodic electropolymerization of the pyrrole-substituted monomer complexes $[Fe[bpypyrr]_3]^{2+}$, $[Ru(bpypyrr)_3]^{2+}$, and $[Ru(bpy)(bpypyrr)_2]^{2+}$ is described, where bpypyrr = 5-(*N*-pyrrolylmethyl)-2,2′-bipyridine and bpy = 2,2′-bipyridine. The stable polymeric thin films have been studied with cyclic voltammetry and chronoamperometry and characterized with ESCA. The iron film has a conductivity of ca. $3 \times 10^{-5}\ \Omega^{-1}\ cm^{-1}$, and charge transport occurs through the films with $D_{ct} = 5 \times 10^{-10}\ cm^2\ s^{-1}$. Electron transfer to solution species may occur either via diffusion through the polymer matrix or via redox conduction through the film. The films possess redox conductivity, which permits sustained film growth.

The modification of electrode surfaces with thin films of electroactive materials has attracted considerable interest recently due to the wealth of potential applications in electrochromic devices, in lightweight batteries, and in the fabrication of molecular electronic devices.[1] Considerable attention has been paid to the formation of redox polymers by the cathodic electropolymerization of transition-metal complexes containing vinyl groups.[2] The resultant films are redox conductors.[3] Anodic electropolymerization of substituted pyrroles or thiophenes produces a doped polymer with high electronic conductivity.[4] In the search to prepare a metallopolymer film that is both a redox and electronic conductor, the functionalized pyrrole ligand 5-(*N*-pyrrolylmethyl)-2,2′-bipyridine (bpypyrr, **1**) has been prepared containing a bipyridyl subunit.[5] This ligand may be used to complex a series of different transition-metal ions. However, there have been relatively few reports of the anodic electropolymerization of functionalized transition-metal complexes.[7]

Recently some related pyrrole-substituted ruthenium complexes have been reported and their electrochemical preparation and photoresponse described.[6] We report the synthesis and oxidative polymerization of the iron and ruthenium complexes of the functionalized pyrrole **1**, the electrochemical and surface characterization of the resultant thin films, and studies which suggest that sustained film growth may occur via a redox conduction mechanism.

Results and Discussion

(a) Synthesis. The pyrrole ligand **1** (bpypyrr) was prepared by reaction of 5-methyl-2,2′-bipyridine[8] with *N*-bromosuccinimide to yield the corresponding bromomethyl derivative. *N*-Alkylation of pyrrole with the bromomethyl compound was effected under phase-transfer conditions to give **1** in 67% yield. The dicationic $[Fe(bpypyrr)_3]^{2+}$ (**2**) and $[Ru(bpypyrr)_3]^{2+}$ (**3**) complexes were prepared according to literature procedures,[9] and the mixed ruthenium complexes $[Ru(bpy)(bpypyrr)_2]^{2+}$ (**4**) and $[Ru(bpy)_2(bpypyrr)]^{2+}$ (**5**) were prepared by using established methods.[2b,10] The copper complex $[Cu(bpypyrr)_2]^{2+}$ (**6**) was also synthesized by a conventional route.[11] The iron and ruthenium complexes **2** and **3** exist as two octahedral diastereoisomers, *mer* and *fac*, each of which is chiral. Separate ^1H NMR signals were observed for the two diastereomers, being most apparent on observation of the pyrrole H-2 and H-3 signals and the bipyridine H-6 resonance. Spectra of the ligand **1** and the iron complex **2** are compared in Figure 1. The *fac* isomer has C_3 symmetry, so that the three pyrrole groups are homotopic and therefore the three pairs of H-2 and H-3 protons resonate as single multiplets. For the *mer* isomer, which lacks any C_n axes, separate signals are seen for each of the three diastereotopic (bpypyrr) ligands at pyrrole H-2 and H-3 and bipyridine H-6. The relative ratio of the two diastereomers was 1.8:1 for **2** and 1.05:1 for **3**. These air-stable complexes, **2**–**6**, may also be conveniently characterized by positive ion fast atom bombardment mass spectrometry. A representative isotope pattern for **3** is shown in Figure 2, showing excellent agreement between calculated and observed intensities.

Table I. Deposition Efficiency for $[[Fe(bpypyrr)_3]^{2+}]_n$[a]

CPE time, min	% efficiency	CPE time, min	% efficiency
0.5	88.5	4.0	53.3
1.0	73.6	8.0	41.5
2.0	61.8		

[a] For deposition onto a glassy-carbon electrode at +1.3 V.

(b) Electrochemistry. A single-sweep cyclic voltammogram, between −0.2 and +1.5 V, of a solution of $[Fe(bpypyrr)_3]^{2+}$ (**2**) showed that the irreversible pyrrole oxidation and the reversible Fe(II)/Fe(III) oxidation occur at similar electrode potentials. By continuous cycling, sustained film growth took place with platinum, glassy-carbon, or SnO_2 electrodes. As polymer is deposited onto the electrode surface, the CV response quickly is dominated by the contribution from the polymer itself, this being reversible one-electron Fe(II)/Fe(III) oxidation/reduction.[23] Under the experimental conditions used, approximately 25 monolayers are deposited in the first cycle (assuming 10^{-10} mol $cm^{-2} \approx 1$ monolayer) and thereafter the anodic and cathodic peak currents quickly become similar in size. A typical cyclic voltammogram showing film growth at a glassy-carbon electrode is shown in Figure 3. The observed responses are nearly Nernstian in

(1) (a) Albery, W. J.; Hillman, A. R. *Annu. Rep. Prog. Chem., Sect. C* **1981**, *78*, 377–437. (b) Pickup, P. G.; Murray, R. W. *J. Am. Chem. Soc.* **1983**, *105*, 4510. (c) Amatore, C.; Saveant, J. M.; Tessier, D. *J. Electroanal. Chem. Interfacial Electrochem.* **1983**, *147*, 39. (d) Anson, F. C.; Ohsaka, T.; Saveant, J. M. *J. Phys. Chem.* **1983**, *87*, 640. (e) Kittlesen, G. P.; White, H. S.; Wrighton, M. S. *J. Am. Chem. Soc.* **1985**, *107*, 7373.
(2) (a) Abruna, H. D.; Denisevich, P.; Umana, M.; Meyer, T. J.; Murray, R. W. *J. Am. Chem. Soc.* **1981**, *103*, 1. (b) Calvert, J. M.; Schmehl, R. H.; Sullivan, B. P.; Facci, J. S.; Meyer, T. J.; Murray, R. W. *Inorg. Chem.* **1983**, *22*, 2151.
(3) Denisevich, P.; Willman, K. W.; Murray, R. W. *J. Am. Chem. Soc.* **1981**, *103*, 4727–4737.
(4) (a) Diaz, A. F.; Kanazawa, K. K.; Logan, J. A.; Salmon, M.; Fajardo, O. *J. Electroanal. Chem. Interfacial Electrochem.* **1981**, *129*, 155. (b) Garnier, F.; Tourillon, G. *J. Electroanal. Chem. Interfacial Electrochem.* **1983**, *148*, 299.
(5) Eaves, J. G.; Munro, H. S.; Parker, D. *J. Chem. Soc., Chem. Commun.* **1985**, 684.
(6) (a) Cosnier, S.; Deronzier, A.; Moutet, J. C. *J. Electroanal. Chem. Interfacial Electrochem.* **1985**, *193*, 193. (b) Cosnier, S.; Deronzier, A.; Moutet, J. C. *J. Phys. Chem.* **1985**, *89*, 4895.
(7) (a) Ellis, C. D.; Margerum, L. D.; Murray, R. W.; Meyer, T. J. *Inorg. Chem.* **1983**, *22*, 1283. (b) Calvert, J. M.; Peebles, D. L.; Nowak, R. J. *Inorg. Chem.* **1985**, *24*, 3111. (c) Macor, K. A.; Spiro, T. E. *J. Am. Chem. Soc.* **1983**, *105*, 5601. (d) Eaves, J. E.; Munro, H. S.; Parker, D. *Synth. Met.* **1986**, *16*, 123.
(8) Huang, T. L. J.; Brewer, D. G. *Can. J. Chem.* **1981**, *59*, 1689.
(9) (a) Burstall, F. H.; Nyholm, R. S. *J. Chem. Soc.* **1952**, 3570. (b) Braddock, J. N.; Meyer, T. J. *J. Am. Chem. Soc.* **1973**, *95*, 3158.
(10) (a) Krause, R. A. *Inorg. Chim. Acta* **1977**, *22*, 209. (b) Sullivan, B. P.; Salmon, D. J.; Meyer, T. J. *Inorg. Chem.* **1978**, *17*, 3334.
(11) Hall, J. R.; Litzow, M. R.; Plowan, R. H. *Aust. J. Chem.* **1965**, *18*, 1331.

0020-1669/87/1326-0644$01.50/0

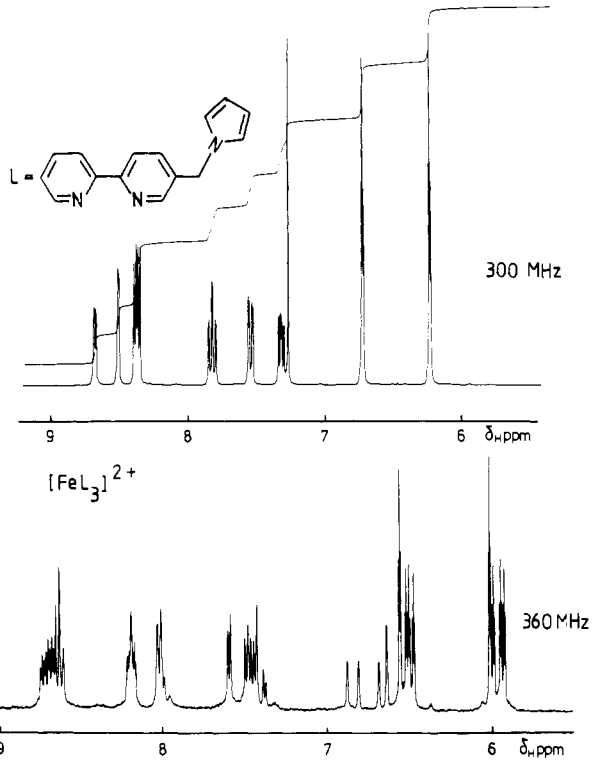

Figure 1. ^1H NMR spectra of the ligand bpypyrr (**1**) in $CDCl_3$ and of the iron complex $[Fe(bpypyrr)_3]^{2+}$ (**2**) in Me_2CO-d_6.

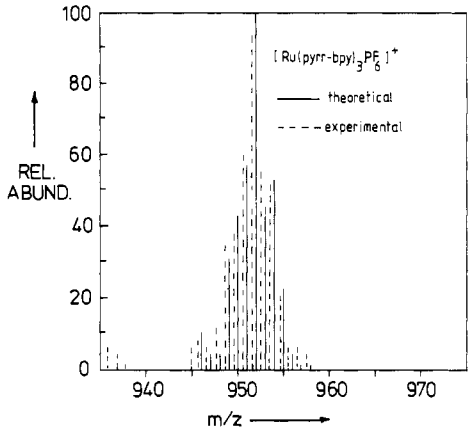

Figure 2. Positive ion fast atom bombardment mass spectrum for $[Ru(bpypyrr)_3]^{2+}$ recorded for a dithioethanol matrix at 8 keV with fast argon atoms.

character for surface-immobilized species, as deduced from the 20-mV peak splitting, E_{fwhm} = 150 mV, and the stable symmetrical peak shape.[12] Both $[Ru(bpypyrr)_3]^{2+}$ (**3**) and $[Ru(bpy)(bpypyrr)_2]^{2+}$ (**4**) could similarly be electrooxidatively polymerized in 0.1 M Bu_4NClO_4 solution, onto the surface of an electrode, by cycling the applied potential between −0.2 and +1.6 V. Characteristic Ru(II)/Ru(III) couples were observed at +1.32 and +1.30 V for **3** and **4**, respectively. In contrast, $[Ru(bpy)_2(bpypyrr)]^{2+}$ was not polymerized by either repeated cycling or use of controlled-potential electrolysis at +1.6 V. The polymerizability of the monomers decreased in the order **2** > **3** > **4** ≫ **5**. The greater ease of polymerization of monomers with increasing number of polymerizable groups has previously been noted in the reductive electropolymerization of vinyl–metal bipyridyl complexes.[2b]

Controlled-potential electrolysis at +1.3 V of $[Fe(bpypyrr)_3]^{2+}$, in acetonitrile solution 0.1 M in Bu_4NClO_4, produced even, red

(12) Brown, A. P.; Anson, F. C. *Anal. Chem.* **1977**, *49*, 1589.

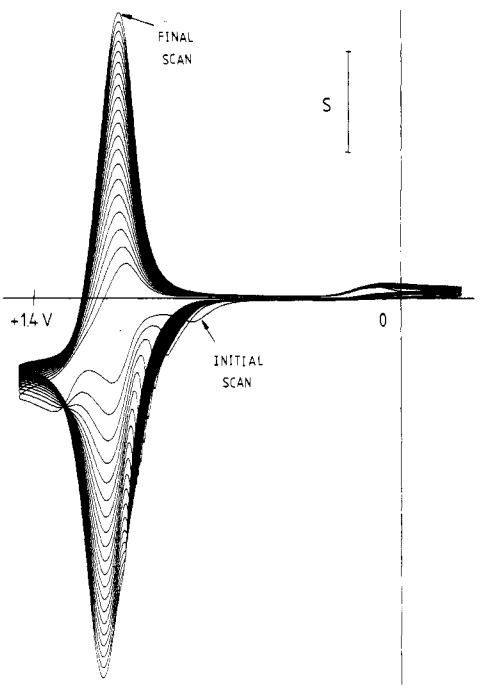

Figure 3. Cyclic voltammogram showing deposition of $[[Fe(bpypyrr)_3]^{2+}]_n$ onto a glassy-carbon electrode (S = 200 μA cm^{-2}, v = 50 mV s^{-1}).

electrode deposits. The deposited films were insoluble in common organic solvents. The deposit formed on a conducting tin oxide coated Pyrex glass electrode appeared red in transmitted light. The visible absorption band appeared at 530 nm, at the same wavelength as for the monomer in solution, suggesting that the metal bipyridyl complex is incorporated intact in the deposited thin film. Deposition efficiencies were calculated from the ratio of the number of moles of monomer deposited on the electrode surface (determined by CV) to the number of moles of monomer oxidized. The number of electrons, n, involved in the film-forming process was taken to be 8. This figure takes account of the irreversible two-electron oxidation of each pyrrole ring, the reversible one-electron oxidation of the Fe(II)/Fe(III) couple, and the oxidative doping level of one electron lost per monomer (as determined by ESCA). The variation of deposition efficiency with CPE deposition time is shown in Table I. The deposition efficiency decreases with increasing deposition time, although this is not caused by oxidative degradation of the films. No oxidized, paramagnetic iron species were observed in the Fe $2p_{3/2}$ ESCA spectra of films of polymerized $[Fe(bpypyrr)_3]^{2+}$ ($[[Fe(bpypyrr)_3]^{2+}]_n$ irrespective of deposition time. The reason for the diminution of deposition efficiency is not clear. A possible explanation is that there is a progressive change in deposition mechanism. At short deposition times (thin films), deposition may occur following diffusion of $[Fe(bpypyrr)_3]^{2+}$ monomers to the growing film/electrode interface where monomer oxidation occurs, which is followed by an efficient polymer incorporation process due to the encapsulation of the oxidized monomer by the growing polymer. At longer CPE times, the diffusional pathway is disfavored and most monomer oxidation may occur via redox conduction through the growing polymer film interface, where the formation of smaller oligomers, which may diffuse into solution, is more likely. When films of $[[Fe(bpypyrr)_3]^{2+}]_n$ are formed by continually cycling the applied potential, the amount of material deposited similarly does not increase linearly with cycle number but slows progressively. The extent of $[[Fe(bpypyrr)_3]^{2+}]_n$ deposition vs. deposition time is shown in Figure 4. Since $[[Fe(bpypyrr)_3]^{2+}]_n$ may be deposited by potential cycling as well as by CPE, it was possible to determine whether or not deposition continues on the electrode surface during CV, at potentials less positive than E^ϕ for Fe(II)/Fe(III).

Also shown in Figure 4, therefore, is a plot of Γ_{app} (determined from normalized CV peak areas) against the time spent at a

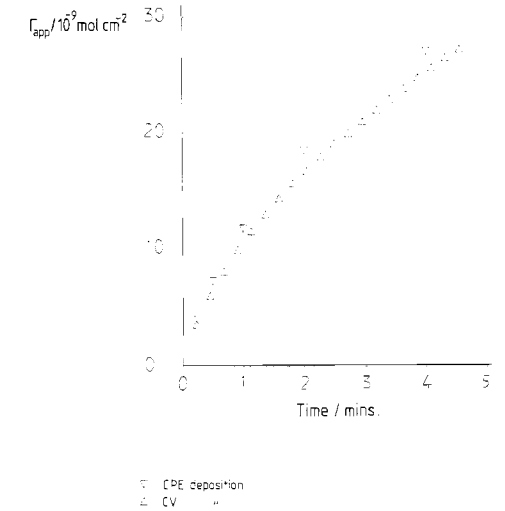

Figure 4. Plot of extent of $[[Fe(bpypyrr)_3]^{2+}]_n$ deposition vs. oxidation time.

potential greater than E^{φ} for Fe(II)/Fe(III), for a film grown during CV. The agreement between the two curves in Figure 4 is good, indicating that deposition occurs only during the period when the monomer may be oxidized. Such a result is consistent with a growth mechanism—similar to that defined for polypyrrole—in which highly reactive radical cations are the key polymer-building species. If a chain propagation mechanism were controlling deposition, then some film formation might occur during the CV "off time". This is evidently not the case.

Films of $[[Fe(bpypyrr)_3]^{2+}]_n$ exhibit high stability toward electrochemical cycling between the Fe(II) and Fe(III) states. Negligible loss of integrated peak current was typically observed after 200 cycles, at 50 mV s^{-1}, between −0.2 and +1.5 V. During this treatment, the film spent approximately 46 min in the oxidized state. Similar high stabilities have been reported for $[[Fe(vbpy)_3]^{2+}]_n$.[13] The stability of a $[[Fe(bpypyrr)_3]^{2+}]_n$-modified electrode toward storage in air was tested. The film was stored in the Fe(II) form. Immediately after deposition, the cyclic voltammogram in monomer-free electrolyte revealed a prepeak to the main oxidation wave (Figure 5). After 5–8 cycles this prepeak merges with the main wave. Its origin is unclear, but similar effects have previously been reported.[13,14] For subsequent CV tests, a different initial response was observed. Over the first 5–10 cycles, the peak current grew and the peak splitting decreased from an initial value of 220 mV to 50 mV on the third cycle and quickly reached a limiting value of 35 mV. During this process the integrated peak current remained constant. It seems likely that egress of dopant anions occurs during storage, as has been reported for polypyrrole[15] and the $[[M(vbpy)_3]^{2+}]_n$ films.[13] Although a slow decrease in CV peak current was observed with storage time, 70% of the electroactivity was retained 75 days after film preparation. There is no evidence that storage of the film produces any perturbation to the charge-transport kinetics since the CV splitting and the peak fwhm remained constant at each weekly test.

The polymerized $[Ru(bpypyrr)_3]^{2+}$ (**3**) and $[Ru(bpy)(bpypyrr)_2]^{2+}$ films were less stable toward oxidative cycling than the iron analogue. For example, 9% of the integrated anodic peak current was lost after cycling a film of $[[Ru(bpypyrr)_2(bpy)]^{2+}]_n$ 56 times between −0.2 and +1.55 V at 50 mV s^{-1}. Oxidative stabilities both superior and inferior to these have been described for electrodeposited ruthenium bipyridyl or pyridyl complexes.[7b,13] For a film of $[[Ru(bpypyrr)_3]^{2+}]_n$, ca. 10% of its electroactivity was lost after 13-day storage in air, in the dark. The CV peak

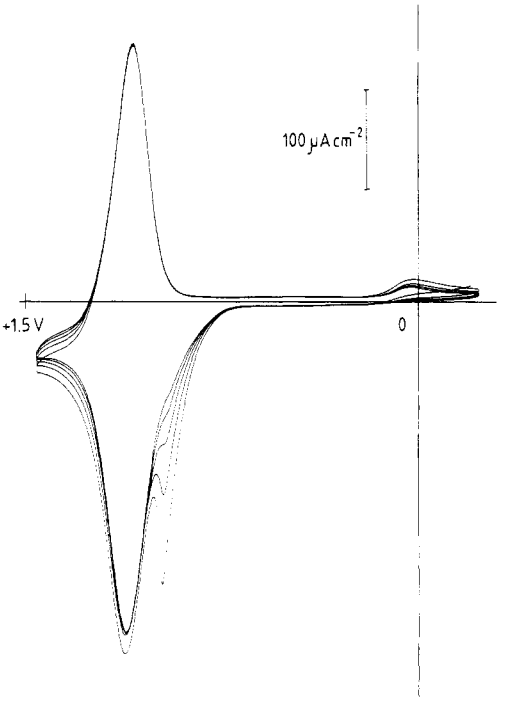

Figure 5. Cyclic voltammogram of $[[Fe(bpypyrr)_3]^{2+}]_n$-modified electrode in CH_3CN/0.1 M Bu_4NClO_4 (v = 50 mV s^{-1}).

splitting and peak width were unchanged during this period. Both the polyruthenium and the polyiron films were unstable toward reductive cycling between 0 and −1.7 V. A potential excursion between 0 and −1.7 V gives rise to a large current spike at ca. −1.2 V. Subsequent anodic scans reveal that all of the M(III)/M(II) electroactivity is lost, and ESCA confirms that after this treatment and exposure to air all the iron or ruthenium in the film has been irreversibly oxidized to the +3 state. Thus for the degraded iron film, one broad Fe $2p_{3/2}$ signal was observed centered at 711.8 eV. Moreover, a large Pt_{4f} signal from the underlying electrode was detected, indicating that the remaining film was only a few nanometers thick.

Plots of anodic peak current against sweep rate were linear for thin films (i.e. $\Gamma_{app} \approx 4 \times 10^{-9}$ mol cm^{-2}) of $[[Fe(bpypyr)_3]^{2+}]_n$, $[[Ru(bpypyrr)_3]^{2+}]_n$, and $[[Ru(bpy)(bpypyrr)_2]^{2+}]_n$. Such behavior is expected for a surface-immobilized electroactive film sufficiently thin for all of the redox sites within the film to undergo oxidation and reduction during one potential cycle. As the film thickness was increased, deviations from linearity became more pronounced and occurred at slower sweep rates. This occurs due to the onset of rate-limiting charge transport through the film, as film thickness increases.[16] The variation of peak splitting and anodic peak fwhm with sweep rate and film thickness is given in Table II. The peak splitting increases for the thicker films at a given sweep rate. A loss of peak symmetry, manifested as a diffusional tail, accompanied the increase in peak splitting.

Potential-step chronoamperometry was used to determine the effective diffusion coefficient, D_{ct}, for charge transport. Several films of $[[Fe(bpypyrr)_3]^{2+}]_n$, deposited onto a platinum electrode to a coverage of ca. 1.2×10^{-8} mol cm^{-2}, were examined individually. Reproducible plots of anodic current vs. $t^{-1/2}$ were obtained, for a given film, upon application of a 0 to +1.6 V potential step. The slope of the linear portion of the plot was measured and D_{ct} calculated from the Cottrell equation by analyzing the linear portion of the plot. The slope of the plot, $nFAD_{ct}{}^{1/2}/\pi^{1/2}$ typically gave $D_{ct}{}^{1/2} = 2.8 \times 10^{-8}$ mol cm^2 s$^{1/2}$. Assuming a redox site concentration of 1.4×10^{-3} mol cm^{-3} (based on an assumed density of 1.35 g cm^{-3} and using the monomer molecular weight of 961), D_{ct} is calculated to be 4.9×10^{-10} cm^2 s^{-1}. Such

(13) Denisevich, P.; Abruna, H. D.; Leidner, C. R.; Meyer, T. J.; Murray, R. W. *Inorg. Chem.* **1982**, *21*, 2153.
(14) Bidan, G.; Deronzier, A.; Moutet, J.-C. *Nouv. J. Chim.* **1984**, *8*, 501.
(15) Erlandsson, R.; Inganas, O.; Lundstrom, I.; Salaneck, W. R. *Synth. Met.* **1985**, *10*, 303.
(16) Ghosh, P. K.; Bard, A. J. *J. Electroanal. Chem. Interfacial Electrochem.* **1984**, *169*, 113.

Table II. Electrochemical Data for Polymeric Thin Films (in 0.1 M Et_4NClO_4/MeCN)

electrode	apparent molar coverage Γ_{app}, mol cm^{-2}	sweep rate, mV s^{-1}	peak splitting, mV	anodic peak fwhm, mV
$[[Fe(bpypyrr)_3]^{2+}]_n$	4×10^{-9}	25	10	155
		50	15	155
		100	15	155
		200	20	160
		400	30	160
	1.2×10^{-8}	25	20	170
		50	20	180
		100	40	170
		200	50	165
		400	75	170
	3.7×10^{-8}	10	30	150
		25	65	160
		50	90	170
		100	110	190
		200	130	205
		400	140	210
$[[Ru(bpypyrr)_3]^{2+}]_n$	3.7×10^{-9}	25	25	160
		50	30	170
		100	30	170
		200	30	170
		200	30	170
		400	30	185
$[[Ru(bpy)(bpypyrr)_2]^{2+}]_n$	3.8×10^{-9}	25	20	130
		50	20	140
		100	30	140
		200	30	140
		400	30	150

a figure is in close agreement to that determined for $[[Ru(vbpy)_3]^{2+}]_n$[3] (1.6×10^{-10} cm^2 s^{-1}) and those of other electrochemically polymerized films of vinyl monomers.[7b,17]

(c) Conductivity and Surface Analysis. Reproducible dry-state conductivity measurements were recorded for films of $[[Fe(bpypyrr)_3]^{2+}]_n$, as defined in the Experimental Section. The even films of $[[Fe(bpypyrr)_3]^{2+}]_n$ tested were thick enough to be colored but did not display interference patterns with visible light. Assuming a film thickness of 10^3 nm (see Experimental Section), a conductivity of 3×10^{-5} Ω^{-1} cm^{-1} was obtained for several separate samples. Such a conductivity value is comparable to that of some *N*-alkylpyrroles[18] and is considerably higher than that obtained for the electronically insulating films derived from vinyl monomers.[3]

The C 1s, N 1s, Fe 2p, and Cl 2p ESCA spectra for a film of $[[Fe(bpypyrr)_3]^{2+}]_n$ formed in CH_3CN/0.1 M Bu_4NClO_4 are shown in Figure 6. The iron $2p_{3/2}$ signal is a single sharp peak (fwhm = 1.3 eV) centered at 709.3 eV, which is the same binding energy for the monomer Fe $2p_{3/2}$ signal. The narrowness of the peak width is consistent with a film in which all of the iron is present in a low-spin d^6 configuration. It is unambiguously evident that the iron(II) tris(bipyridyl) unit remains intact upon electropolymerization. The observed Cl 2p signal was consistent with ClO_4^- binding energy, and the amount of oxygen detected in the film also agreed with a ClO_4^- anion being the only oxygen-containing species. The N/Cl stoichiometry was 3.0, and that of Cl/Fe was also 3.0. Such ratios are indicative of film oxidation to a level of one positive charge per monomeric unit, or a polypyrrole dopant oxidation level of 33%. The N 1s spectrum is similar to that of the monomer, and the pyrrole and bipyridyl nitrogens were not resolved. Distinct "shake-up" satellites were observed in the C 1s and N 1s spectra. The position and intensity of the C 1s "shake-up" are similar to those found for the monomer and are diagnostic of the localized unsaturation of the bipyridyl system.

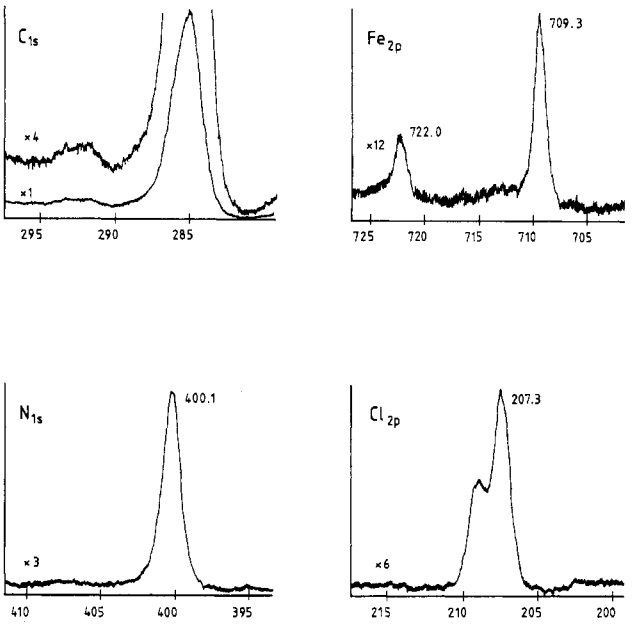

Figure 6. ESCA spectra for a film of $[[Fe(bpypyrr)_3]^{2+}]_n$ formed in CH_3CN/0.1 M Bu_4NClO_4 solution. Binding energies are in eV relative to C 1s at 285 eV.

C 1s (and Ru $3d_{5/2}$), N 1s, and Cl 2p ESCA spectra for $[[Ru(bpypyrr)_3]^{2+}]_n$ are shown in Figure 7. Similar spectra were obtained for $[[Ru(bpy)(bpypyrr)_2]^{2+}]_n$. The Ru $3d_{5/2}$ signal is a single sharp peak (fwhm = 1.6 eV) centered at 280.9 eV, which is the same binding energy as for the monomer. Evidently the ruthenium is all present in a low-spin d^6 configuration. A nitrogen to chlorine stoichiometry of 3.2 was observed consistent with a polypyrrole chain oxidation level of 27%. The binding energy and peak width of the Ru $3d_{5/2}$ signal preclude the possibility that this positive charge is associated with the metal.

(d) Cyclic Voltammetry in the Presence of Solution Redox Species. Electrodes coated with films of $[[Fe(bpypyrr)_3]^{2+}]_n$ were examined by cyclic voltammetry in the presence of ferrocene and dichloro-5,6-dicyano-*p*-benzoquinone (DDQ), both of which undergo one-electron oxidation at potentials less positive than that of the Fe(II)/Fe(III) couple (E^{ϕ}_{pol}). In principle, ferrocene and DDQ may be oxidized at the electrode/polymer interface, after diffusion through a continuous polymer film, or at the polymer film/solution interface, a process that requires either redox conduction through the film or an electronically conducting film. In the case of redox-conductivity-mediated electron transfer, *irreversible* oxidation of the solution species will occur at or near E^{ϕ}_{pol}. Oxidation would be rapid and the anodic current appear as a "spike". For electron transfer mediated by an electronically conducting film, *reversible* oxidation will occur at or near E^{ϕ}_{soln}. Electron transfer involving solution species at a redox-polymer-coated electrode at both E^{ϕ}_{pol} and E^{ϕ}_{soln} have previously been reported.[6,19,20]

A cyclic voltammogram for a solution of 10^{-2} M ferrocene at an electrode freshly coated with 1.2×10^{-8} mol cm^{-2} of $[[Fe(bpypyrr)_3]^{2+}]_n$ is shown in Figure 8A. Almost all of the ferrocene oxidation occurs at E^{ϕ}_{soln}, although some oxidation also occurs at E^{ϕ}_{pol}, as seen in Figure 8B, in which the oxidation peak around E^{ϕ}_{pol} is expanded and compared to the polymer peak in inert solvent and electrolyte. The "spiked" form of the ferrocene oxidation is apparent. Similar results were observed for DDQ oxidation. However, one-electron reduction of DDQ was inhibited compared to oxidation. A similar selective inhibition of DDQ reduction has been reported for electrodes coated with 1,1-bis(chloromethyl)ferrocene.[21] Parallel experiments were conducted

(17) Facci, J. S.; Schmehl, R. H.; Murray, R. W. *J. Am. Chem. Soc.* **1982**, *104*, 4959.
(18) Diaz, A. F.; Castillo, J.; Kanazawa, K. K.; Logan, J. A.; Salmon, M.; Fajardo, O. *J. Electroanal. Chem. Interfacial Electrochem.* **1982**, *133*, 233.
(19) Ellis, C. D.; Murphy, W. R.; Meyer, T. J. *J. Am. Chem. Soc.* **1981**, *103*, 7480.
(20) Ikeda, T.; Schmehl, R.; Denisevich, P.; Willman, K.; Murray, R. W. *J. Am. Chem. Soc.* **1982**, *104*, 2683.

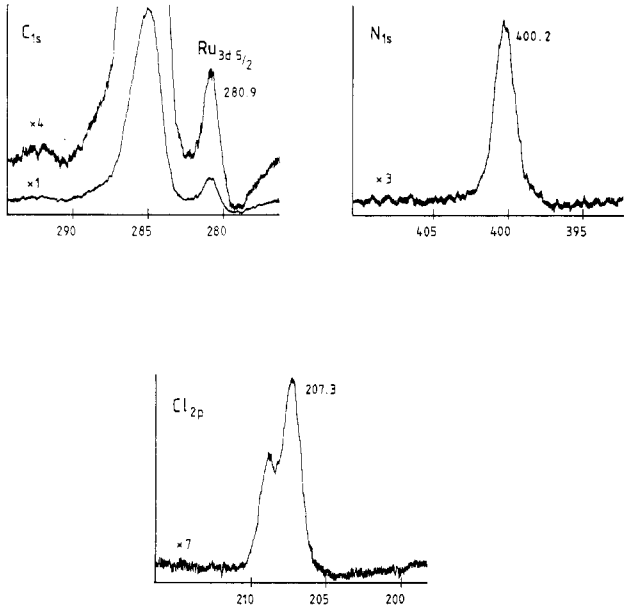

Figure 7. ESCA spectra for a film of $[[Ru(bpypyrr)_3]^{2+}]_n$ formed in $CH_3CN/0.1$ M Bu_4NClO_4 solution.

with an electrode that had been stored for 75 days, during which time the apparent molar coverage decreased from 1.1×10^{-8} to 0.7×10^{-8} mol cm^{-2}. Almost all of the ferrocene oxidation in this case occurred near E^{ϕ}_{pol} (Figure 9), and similar results were obtained with DDQ.

These results suggest that, for an aged electrode, oxidation of solution species is facilitated by redox conduction through the polymer film. Clearly storage of the film produces a change that inhibits oxidation of the solution species at E^{ϕ}_{soln}. It is most unlikely that the freshly prepared films were cracked or contained pinholes and that the aged film was defect-free. Indeed, optical microscopy of films of similar thickness but different age showed them to be smooth, continuous, and defect-free. Moreover, short circuits were not found when measuring conductivities of films of different age.

It appears that the freshly prepared films either permit diffusion of the solution redox species, as suggested by recent work,[6] or have some electronic conductivity. Although polypyrrole is known to lose its electronic conductivity and may undergo some surface degradation upon air storage,[15] this appears not to provide the most reasonable explanation in this case, for the following reasons: (a) no change in the CV characteristics (peak splitting, wave shape, E^{ϕ}) in inert solution was observed for the aged modified electrode compared to the freshly prepared one; (b) if we suppose that films of $[[Fe(bpypyrr)_3]^{2+}]_n$ were initially sufficiently electronically conducting to permit oxidation of solution species at E^{ϕ}_{soln}, it is unlikely that a second oxidation peak at E^{ϕ}_{pol} would also be observed (as is seen in Figure 8B) since both electronic and redox conductivity mediated electron transfers to solution species occur at the film/solution interface; (c) the initial and aged films were of similar thickness.

In summary, for an electrode modified with $[[Fe(bpypyrr)_3]^{2+}]_n$ that has been aged in air, the most likely pathway for oxidation of ferrocene and DDQ in solution is via redox conduction through the film. For a freshly prepared modified electrode, it is probable that oxidation of the solution species occurs at the electrode/polymer interface, following diffusion of these species through the relatively porous polymer lattice. Finally, given that attempts to electropolymerize $[Cu(bpypyrr)_2]^{2+}$ by either CV or bulk electrolysis were unsuccessful, it seems likely that redox conductivity is also essential for sustained film growth with this metal complex system. If a growing film does not possess a sufficiently high electronic conductivity, then redox conductivity is required for film growth. For the iron and ruthenium complexes, the iron(III) and ruthenium(III) centers are capable of inducing polymerization at the film/solution interface by *oxidation* of the pyrrole function. For a $[[Cu(bpypyrr)_2]^{2+}]_n$ film to form, the Cu(III) state must be reversibly formed. No such wave was observed in a cyclic voltammogram of $[Cu(bpypyrr)_2]^{2+}$.

Further work is in progress to develop the scope of the electropolymerization reaction by using copolymerizations with pyrrole monomer and by using β-bpy-substituted pyrrole monomers in order to enhance the intrinsic electronic conductivity of the deposited films.

Experimental Section

General Considerations. All reactions were carried out under a dry argon atmosphere and, where appropriate, in the dark. Proton NMR spectra were recorded on a Bruker WH360 or a Bruker AC250 spectrometer, with chemical shifts given in ppm to higher frequency of Me_4Si. Mass spectra were recorded on a VG 7070E spectrometer fitted with a fast atom bombardment attachment. Visible absorption spectra were recorded on a Pye-Unicam SP8-100 spectrophotometer.

Electrochemical and Conductivity Experiments. A potassium chloride saturated calomel electrode was used as reference. Tetrabutylammonium perchlorate and fluoroborate electrolytes were dried in a vacuum oven prior to use, and all solvents were dried immediately prior to use. Electrode deposits were formed by controlled-potential electrolysis using a Thompson Ministat 251 precision potentiostat and a Fluke 8000A digital multimeter to set the potential and measure the current. For cyclic voltammetric analysis, films were prepared by deposition from solutions that were 2×10^{-3} M in the relevant monomer onto Kel-F-shrouded platinum or glassy carbon disk electrodes. These electrodes were polished with diamond and alumina pastes, washed with distilled water, and dried before use. A platinum-wire counter electrode was used. Cyclic voltammograms were recorded with a BAS CV-5B instrument, and peak areas were determined with an Apple II/e microcomputer with graphics tablet, light pen, and associated software. The areas used in apparent molar coverage calculations were the average of at least five determinations. For chronoamperometry experiments, the Thompson Ministat 251 potentiostat was used to apply a 0 to +1.6 V potential jump to the modified electrode. The current response was measured with use of a small resistance in series with the cell. An analog instrumentation amplifier was used to provide a differential voltage input to a Tektronix 5115 storage oscilloscope, on which the transient response was displayed.

Conductivity measurements were performed on films deposited onto new platinum-flag electrodes. Gold contacts (1.5-mm diameter) were slowly evaporated on top of the films with an Edwards vacuum evaporator. Film resistance measurements were taken with a base contact to the platinum electrode and a "soft" spherical gold probe to the evaporated contact. Film resistance was determined from a plot of applied voltage (Time Electronics 2003S dc voltage supply) against measured current (Keithley 414A picammeter). Several films and several contacts for each film were tested. The film thickness was estimated from the charge passed during electrolysis, the electrode area, the experimentally determined deposition efficiency, and the estimate that 10^{-10} mol cm$^{-2} \approx 1$ monolayer and one monolayer ≈ 10 Å.[22]

Surface Analysis. After preparation, films were washed in electrolyte-free solvent and dried under nitrogen and subsequently under vacuum. A Kratos ES300 electron spectrometer was used to record the ESCA spectra. Coated electrodes were mounted onto a standard Kratos probe tip with double-sided "Scotch" tape. Spectra were recorded with the sample positioned at an angle of 35° with respect to a plane parallel to the location of the electron analyzer slits. Mg Kα X-radiation was used. Binding energies are quoted relative to hydrocarbon C 1s at 285 eV. Surface elemental stoichiometries were obtained from peak area ratios corrected by the appropriate elemental sensitivity factors, determined experimentally from standard samples. Curve fitting of ESCA spectra was performed manually with the graphics software of the Kratos ES300 computer system. A linear background subtraction was used. Gaussian component peaks were used exclusively, and constant peak width (fwhm) was used for all components of any one core-level spectrum.

5-(*N*-Pyrrolylmethyl)-2,2′-bipyridine (1). Freshly recrystallized *N*-bromosuccinimide (1.96 g, 11 mmol) and azobis(isobutyronitrile) (50

(21) Nishihara, H.; Aramaki, K. *J. Chem. Soc., Chem. Commun.* **1985**, 709.

(22) Murray, R. W. *Electroanal. Chem.* **1984**, *13*(3), 235.

(23) The origin of the prewave observed in early scans is unclear: other workers have reported similar phenomena in both related[6] and dissimilar systems.[2] The most anodic peak is seen clearly only in the first scan (Figure 3) and may be pyrrole monomer oxidation. It occurs at a potential similar to that of simple *N*-alkylpyrrole oxidation.

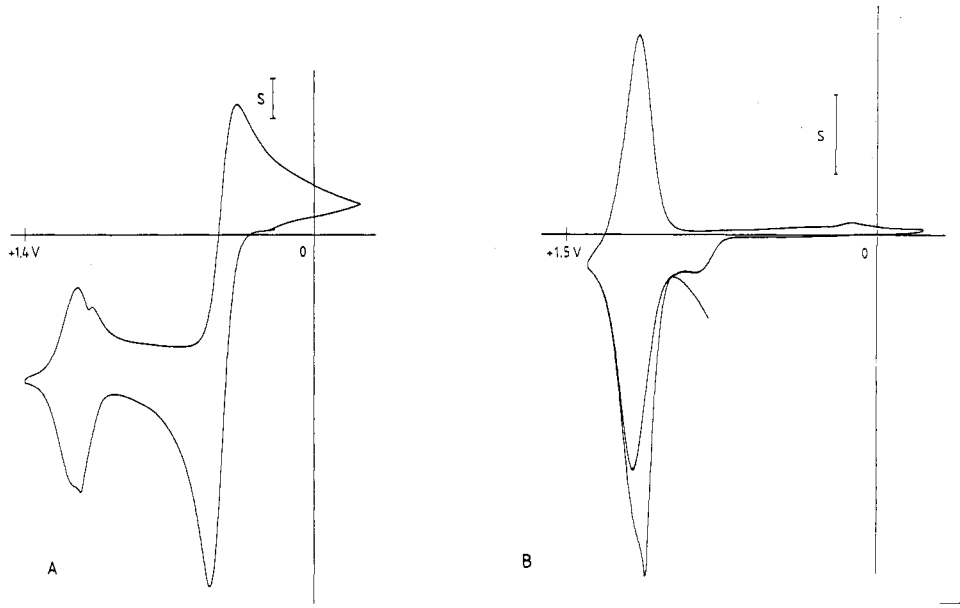

Figure 8. (A) CV of $[[Fe(bpypyrr)_3]^{2+}]_n$-modified electrode in the presence of ferrocene in solution (S = 125 μA cm^{-2}; v = 50 mV s^{-1}). (B) Comparison of the anodic CV wave at E^{ϕ}_{pol} before and after the addition of ferrocene to the electrolyte solution (S = 100 μA cm^{-2}; v = 50 mV s^{-1}).

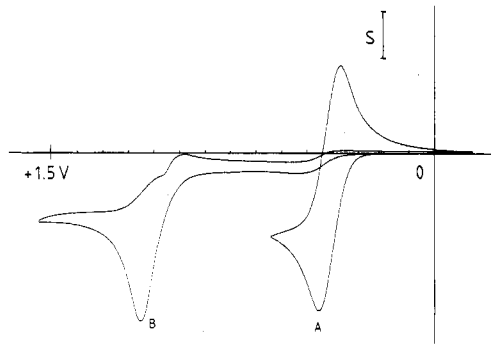

Figure 9. CV response for a ferrocene solution at (A) an uncoated and (B) a 75-day-aged $[[Fe(bpypyrr)_3]^{2+}]_n$-coated electrode (S = 200 μA cm^{-2}; v = 50 mV s^{-1}).

mg) were added to a solution of 5-methyl-2,2′-bipyridine[8] (1.7 g, 10 mmol) in dry tetrachloromethane (100 mL), and the solution was refluxed for 10 h. After it was cooled to 0 °C, the solution was filtered and the solvent removed under reduced pressure to leave a pale yellow oil of 5-(bromomethyl)-2,2′-bipyridine, which was used directly without further purification. MS: m/e 248 (100), 169 (51), 141 (32), 117 (61). To a solution of the crude 5-(bromomethyl)-2,2′-bipyridine (2.48 g, 10 mmol) in dichloromethane (20 mL) was added in sequence aqueous sodium hydroxide solution (50%, 10 mL), tetra-*n*-hexylammonium bromide (50 mg), and pyrrole (670 mg, 10 mmol). The mixture was stirred for 8 h at 35 °C and then poured into water (30 mL) and the organic layer separated and washed with water (3 × 10 mL). After removal of solvent under reduced pressure the residue was chromatographed on neutral alumina with toluene to yield **1** (1.57 g, 67%) as a colorless solid, which was washed with cold hexane (3 × 10 mL) and dried under vacuum; mp 87–88 °C. ^{1}H NMR ($CDCl_3$): 5.15 (s, 2 H); 6.22 (dd, 2 H); 6.72 (dd, 2 H); 7.31 (td, 1 H); 7.53 (dd, J = 8.2, 2.3 Hz, 1 H); 7.81 (td, J = 7.8, 1.8 Hz, 1 H); 8.35 (d, J = 7.8 Hz, 1 H); 8.37 (d, J = 8.1 Hz, 1 H); 8.50 (br d, J = 1.8 Hz, 1 H); 8.68 (m, 1 H). MS (NH_3, CI): m/e 236 (100), 235 (41), 170 (39), 169 (51). Anal. Calcd for $C_{15}H_{15}N_3$: C, 76.6; H, 5.53; N, 17.9. Found: C, 76.3; H, 5.61; N, 17.7.

Syntheses of Complexes. The iron complex was prepared according to a literature procedure,[9] and the ruthenium and copper complexes were prepared from $Ru(bpy)_2Cl_2\cdot 2H_2O$,[10b] $Ru(bpy)Cl_4$,[10a] $RuCl_3\cdot 3H_2O$, or copper perchlorate according to established methods.[9b,11]

Tris[5-(*N*-pyrrolymethyl)-2,2′-bipyridine]iron Tetrafluoroborate (2). To a solution of ferrous sulfate (0.2 g) in water (10 mL) was added sodium tetrafluoroborate (0.3 g) and the ligand **1** (175 mg, 0.74 mmol). The mixture was refluxed for 2 h and on cooling yielded red crystals of the salt, which were collected by filtration, washed with cold water, and dried under vacuum (194 mg, 80%). ^{1}H NMR ($(CD_3)_2CO$): 5.13–5.25 (m, 6 H); 5.91, 5.95, 5.99, 6.01 (dd + dd + dd + dd, 6 H); 6.48, 6.50, 6.52, 6.56 (dd + dd + dd + dd, 6 H); 6.64, 6.69, 6.81, 6.88 (s + s + s + s, 3 H); 7.49–7.60 (m, 6 H); 8.03 (m, 3 H), 8.18 (m, 3 H); 8.60–8.75 (m, 6 H). MS (FAB, thiodiethanol): m/e 848 ($M^+ - BF_4$), 761 ($M^+ - 2\ BF_4$). Anal. Calcd for $B_2C_{45}H_{39}F_8FeN_9\cdot 2H_2O$: C, 55.6; H, 4.43; N, 13.0. Found: C, 55.8; H, 4.21; N, 12.6.

Tris[5-(*N*-pyrrolylmethyl)-2,2′-bipyridine]ruthenium Hexafluorophosphate (3). To a solution of ruthenium trichloride (111 mg, 0.42 mmol) in dry dimethylformamide (10 mL) was added the ligand **1** (350 mg, 1.49 mmol), and the solution was refluxed for 45 h in the dark, after which time only a single visible absorption band at 450 nm was discerned. The cooled solution was added dropwise with stirring to a solution of ammonium hexafluorophosphate (0.3 g) in water (20 mL) to yield an orange precipitate. After repeated washing with water, the complex **3** was collected by centrifugation and dried in vacuo (375 mg, 81%). ^{1}H NMR ($(CD_3)_2CO$): 5.17–5.24 (m, 6 H); 5.92, 5.94, 5.98, 6.02 (dd + dd + dd + dd, 6 H); 6.48, 6.51, 6.52, 6.56 (dd + dd + dd + dd, 6 H); 6.75, 6.95, 7.03, 7.18 (s + s + s + s, 3 H); 7.45–7.52 (m, 3 H); 7.75–8.13 (m, 6 H); 8.16–8.22 (m, 3 H); 8.66–8.74 (m, 6 H). MS (FAB, thiodiethanol): m/e 952 ($M^+ - PF_6$), 807 ($M^+ - 2\ PF_6$). Anal. Calcd for $C_{45}H_{39}F_{12}N_9P_2Ru\cdot 3H_2O$: C, 48.4; H, 3.66; N, 11.3. Found: C, 48.1; H, 3.93; N, 11.1.

Bis[5-(*N*-pyrrolylmethyl)-2,2′-bipyridine](2,2′-bipyridine)ruthenium Tetrafluoroborate (4). To a solution of tetrachloro(2,2′-bipyridyl)ruthenate (40 mg, 0.1 mmol) in isopropyl alcohol (5 mL) was added the ligand **1** (90 mg, 0.38 mmol) and the mixture refluxed for 6 h in the dark. After removal of solvent under reduced pressure, the residue was dissolved in water (10 mL) and the solution filtered and added to a solution of sodium tetrafluoroborate (0.3 g) in water (5 mL) to yield an orange precipitate. This was redissolved in dichloromethane (2 mL) and the solution added slowly dropwise with stirring to dry ether (20 mL) to give an orange precipitate, which was filtered and dried in vacuo (58 mg, 65%). ^{1}H NMR (CD_2Cl_2): 5.05–5.15 (m, 4 H); 5.93–6.06 (m, 4 H); 6.45–6.58 (m, 4 H); 6.90–8.40 (m, 22 H). MS (FAB, thiodiethanol): m/e 902 (M^+), 815 ($M^+ - BF_4$), 728 ($M^+ - 2\ BF_4$). Anal. Calcd for $B_2C_{40}H_{34}F_8N_8Ru\cdot 2H_2O$: C, 50.9; H, 4.03; N, 11.9. Found: C, 50.5; N, 11.6; H, 4.31.

[5-(*N*-Pyrrolylmethyl)-2,2′-bipyridine]bis(2,2′-bipyridine)ruthenium Perchlorate (5). To a solution of dichlorobis(2,2′-bipyridine)ruthenium (260 mg, 0.5 mmol) in ethanol (5 mL) was added the ligand **1** (118 mg, 0.5 mmol) and the mixture refluxed in the dark for 20 h. After evaporation to dryness, the residue was redissolved in water (10 mL) and a solution of lithium perchlorate (0.25 g) in water (3 mL) was added slowly to give an orange precipitate. This was redissolved in dry acetone (3 mL) and added dropwise onto ether (25 mL) to give an orange precipitate, which was dried in vacuo (330 mg, 78%). ^{1}H NMR ($(CD_3)_2CO$): 5.22 (dd, 2 H); 6.04 (dd, 2 H); 6.54 (dd, 2 H); 7.23 (br s, 1 H); 7.60 (m, 5 H); 7.8–8.1 (m, 6 H); 8.18 (m, 5 H); 8.73–8.82 (m, 6 H). MS (FAB, thiodiethanol): m/e 748 ($M^+ - ClO_4$), 649 ($M^+ - 2\ ClO_4$). Anal. Calcd for $C_{35}H_{29}Cl_2N_7O_8Ru\cdot H_2O$: C, 48.3; H, 3.56; N, 11.2. Found: C, 48.6; H, 3.81; N, 11.6.

Bis[5-(*N*-pyrrolylmethyl)-2,2′-bipyridine]copper Perchlorate (6). To a solution of copper(II) perchlorate (90 mg, 0.24 mmol) in ethyl acetate

(15 mL) was added the ligand **1** (118 mg, 0.5 mmol) and the solution heated at 60 °C for 30 min. The resultant green-blue precipitate was filtered and recrystallized from hot ethanol to give **6** as a green microcrystalline solid (311 mg, 85%). MS (FAB, thiodiethanol): *m/e* 632 ($M^+ - ClO_4$), 533 ($M^+ - 2\ ClO_4$). Anal. Calcd for $C_{30}H_{26}Cl_2CuN_6O_8$: C, 49.1; H, 3.82; N, 11.5. Found: C, 48.9; H, 3.50; N, 11.1.

Acknowledgment. We thank the SERC for a studentship (J.G.E.) and the Royal Society for funds to aid purchase of the fast atom bombardment mass spectrometric facility.

Contribution from the Department of Chemistry,
University of Alberta, Edmonton, Alberta, Canada T6G 2G2

Hexacoordinate Phosphorus. 4. Preparation and Characterization of Fluoro(pentane-2,4-dionato)(trifluoromethyl)phosphorus(V) Derivatives

Neil Burford, Dietmar Kennepohl, Martin Cowie, Richard G. Ball, and Ronald G. Cavell*

Received July 17, 1986

Fluoro(trifluoromethyl)phosphorus(V) derivatives with the pentane-2,4-dionato ligand (acetylacetone) of the general formula $F_{4-x}(CF_3)_xPOC(CH_3)C(H)C(CH_3)O$ (x = 1-3) and $CH_3(CF_3)_3POC(CH_3)C(H)C(CH_3)O$ have been prepared and compared to the known $F_4P(acac)$ (i.e., x = 0). All are stable crystalline solids with a six-coordinate phosphorus geometry as illustrated by the characteristic high-field ^{31}P NMR chemical shifts and the ^{19}F and ^{31}P coupling constant patterns. The six-coordinate nature of these derivatives is further substantiated by the crystal and molecular structures of $F_2(CF_3)_2POC(CH_3)C(H)C(CH_3)O$ (III) and $F(CF_3)_3POC(CH_3)C(H)C(CH_3)O$ (IV). Crystal data for III: orthorhombic, space group *Pbca* (No. 61), a = 12.323 (4) Å, b = 22.871 (5) Å, c = 7.505 (5) Å, V = 2115 Å^3, Z = 8. Final R and R_w values for III were 0.090 and 0.105, respectively. The molecular structure of III shows that the acac ligand is essentially planar and that the two F and acac substituents lie in the same plane about the six-coordinate phosphorus atom. Crystal data for IV: monoclinic, space group $P2_1/c$ (No. 14), a = 10.218 (1) Å, b = 8.822 (3) Å, c = 13.930 (7) Å, β = 107.21 (3)°, V = 1196 Å^3, Z = 4. Final R and R_w values for IV were 0.047 and 0.070, respectively. The molecular structure of IV shows that the unique F occupies a position perpendicular to the central plane, which comprises two of the CF_3 groups and the two oxygen atoms of the acac ligand. The acac ligand is planar but is folded about the O-O axis by approximately 27° toward the unique fluorine. Infrared, mass, and ultraviolet spectra are reported for the compounds.

Introduction

We have previously described several neutral six-coordinate phosphorus(V) compounds with bidentate carbamate and thiocarbamate substituents.[1-7] Several structural characterizations have clearly demonstrated the six-coordinate geometry, expanding significantly the meager list of neutral λ^6-phosphorane structures. Herein we extend the system to include complexes of the acetylacetonate ligand, the prototypical member of which, $F_4POC(CH_3)C(H)CH_3O$, was synthesized in 1966[8] and structurally characterized in 1978.[9]

Experimental Section

All reactions were carried out in sealed tubes, and standard vacuum line techniques were employed for the manipulation of volatile materials. Diethyl ether was dried before use by distillation over $LiAlH_4$ and chloroform by distillation over P_2O_5. All of the phosphoranes used were prepared by the literature methods.[10,11] Sodium acetylacetonate was prepared from NaOH and acetylacetone in ethanol, and acetylacetone (Aldrich) was used as received. Infrared spectra were obtained as Nujol mulls of the solid samples with CsI plates on a Perkin-Elmer 457 grating spectrometer. Mass spectra were recorded with an AEI MS-9 spectrometer operating at an ionizing voltage of 70 eV. NMR spectra were recorded on solutions of the compound in CD_2Cl_2 or $CDCl_3$. ^1H NMR spectra were measured on a Bruker WP-80 instrument in the continuous-wave mode, and the chemical shifts were measured relative to an external Me_4Si sample. ^{19}F and ^{31}P NMR spectra were recorded on a Bruker WP-400 spectrometer at 376.4 and 161.98 MHz, respectively. Chemical shifts were measured with respect to the heteronuclear ^2D lock signal and converted to the $CFCl_3$ scale in the case of ^{19}F and the H_3PO_4 scale in the case of ^{31}P by means of the appropriate conversion factors. Ultraviolet spectra were recorded in chloroform with a Unicam SP 1700 spectrophotometer. Chemical analyses were determined by Schwarzkopf Microanalytical Laboratory, Woodside, NY 11377.

(1) Preparation of (Pentane-2,4-dionato)tetrafluorophosphorus(V) (I). $F_4POC(CH_3)C(H)C(CH_3)O$ was prepared by the literature[8,9] method. The compound was recrystallized from $CHCl_3$; mp 82-83 °C. Anal. Calcd for $C_5H_7O_2F_4P$: C, 29.14; H, 3.42; F, 36.88; P, 15.03. Found: C, 29.39; H, 3.46; F, 36.86; P, 15.01. Principal mass spectral peaks: (*m/e* (relative intensity, percent of strongest peak) [identity]): 206 (7.5) [M]; 191 (5.5) [$M - CH_3$]; 147 (9.9) [$FPOC_4H_5$]; 107 (100.0) [F_4P]; 87 (7.0) [POC_3H_4]; 43 (41.1) [C_2H_3O].

(2) Preparation of (Pentane-2,4-dionato)(trifluoromethyl)trifluorophosphorus(V) (II). CF_3PF_4[10] (1.771 g, 10.01 mol) and acetylacetone (0.993 g, 9.93 mmol) were combined under vacuum with 10 mL of diethyl ether in a sealed tube. The mixture was allowed to warm very slowly (in a cold Dewar) overnight to room temperature. This reaction is exothermic. (At higher temperature CF_3PF_4 decomposes to PF_5,[10] which in turn yields $F_4P(acac)$.) The reaction yielded a yellow Et_2O solution and a yellow oil, which was immiscible with the solution. This oil was separated from the Et_2O solution in a separatory funnel, and it was then treated with several portions of Et_2O until only a small residue of the oily material remained. All of these Et_2O aliquots were combined and the solvent removed in vacuo to leave a pale yellow oily material. Adding a few drops of CCl_4 to this material followed by cooling yielded a small amount of crystalline material. These crystals were oily and unsuitable for chemical analysis. By means of ^{19}F, ^1H, and ^{31}P NMR and UV spectra the crystalline product has however been identified as a mixture of the two structural isomers of $F_3(CF_3)POC(CH_3)C(H)C(CH_3)O$ (II). An NMR spectrum of the above reaction mixture before

(1) The, K. I.; Vande Griend, L.; Whitla, W. A.; Cavell, R. G. *J. Am. Chem. Soc.* **1977**, *99*, 7379.
(2) Cavell, R. G.; The, K. I.; Vande Griend, L. *Inorg. Chem.* **1981**, *20*, 3813.
(3) Cavell, R. G.; Vande Griend, L. *Inorg. Chem.* **1983**, *22*, 2066.
(4) Cavell, R. G.; Vande Griend, L. *Phosphorus Sulfur* **1983**, *18*, 89.
(5) Cavell, R. G.; Vande Griend, L. *Inorg. Chem.* **1986**, *25*, 4699.
(6) Ziegler, M. L.; Weis, J. *Angew. Chem., Int. Ed. Engl.* **1969**, *8*, 445.
(7) John, K. P.; Schmutzler, R.; Sheldrick, W. S. *J. Chem. Soc., Dalton Trans.* **1974**, 1841.
(8) Brown, N. M. D.; Bladon, P. *J. Chem. Soc., Chem. Commun.* **1966**, 304.
(9) Sheldrick, W. S.; Hewson, M. J. C. *Z. Naturforsch., B: Anorg. Chem., Org. Chem.* **1978**, *33B*, 834.
(10) Mahler, W. *Inorg. Chem.* **1963**, *2*, 230.
(11) The, K. I.; Cavell, R. G. *Inorg. Chem.* **1977**, *16*, 2887.

0020-1669/87/1326-0650$01.50/0